RADAR RESPONSE APPROXIMATIONS FOR BURIED PLASTIC LANDMINES

Friedrich Roth[a], Piet van Genderen[a], Michel Verhaegen[b]
[a]International Research Centre for Telecommunications-transmission and Radar (IRCTR)
[b]Control Laboratory
Faculty of Information Technology & Systems, Delft University of Technology
P.O. Box 5031, 2600 GA Delft, The Netherlands
f.roth@irctr.tudelft.nl p.vangenderen@irctr.tudelft.nl m.verhaegen@its.tudelft.nl

ABSTRACT

This paper analyzes the early-time radar response of buried penetrable targets such as plastic landmines. The Born approximation is used to derive simple analytical expressions relating target and soil properties to the early-time response. Understanding these dependencies is crucial for target identification under varying soil conditions. The derived expressions include the transfer function and the impulse response of a penetrable target embedded in an unbounded homogeneous lossy medium and illuminated by a uniform plane wave. Using a truncated circular cylinder having the dimensions of a PMA-3 mine as an example, the early time responses predicted by the Born approximation are compared against responses obtained by three-dimensional finite-difference time-domain (FDTD) simulations. The results demonstrate that with the Born approximation it is possible to predict the general shape of the target response, i.e. the number of amplitude peaks, as well as the amplitudes of those peaks that relate to backscatter from the top of the example target. To improve the fit between the predicted and simulated responses, two phenomenologically motivated modifications to the early-time response expressions are proposed. The modified expressions are able to accurately predict not just the general shape of the early-time response, but also the influence of the host medium conductivity on the target impulse response.

Key words: ground penetrating radar, buried plastic landmines, identification, early-time response, Born approximation, impulse response, transfer function, FDTD simulation

INTRODUCTION

A key feature of Ground Penetrating Radar (GPR) as a landmine detection sensor is that it provides a target scattering signature, which can be used for object identification in addition to detection. The scattering signature contains two components, namely the early-time (forced) and late-time (natural) response of the target (Kostylev, 1994). The early-time response has a finite duration and is formed while the incident wave passes through and along the outside of the target. The late-time response refers to the target's natural modes, which build up after the target has been illuminated by the incident wave. Landmine and unexploded ordnance identification based on complex natural resonances (CNR) computed from the late-time response has been the topic of extensive research throughout the years (see for example: Baum, 1999, Chen and Peters, 1997). The motivation to work with CNR stems from the fact that the resonances are target orientation independent and lead to a small number of characterizing parameters. However, it was found that for buried targets the resonances are highly damped compared to the free-space case and thus discrimination becomes difficult. This is especially true for plastic landmines, whose late-time response is relatively weak even in air. Hence for plastic landmines it seems more appropriate to work with the early-time response, which is relatively strong compared to the late-time response.

The early-time response carries information about both the shape and the internal structure of the landmine. Consequently, the early-time response is a valuable target signature and can be used for landmine identification. However, it is well known that the early-time response is dependent not only on the electromagnetic properties of the landmine, but also on those of the soil in which the landmine is buried. In addition, the early-time response is dependent on the landmine's orientation with respect to the incident and scattering directions. Hence, in order to fully exploit the early-time response it is important to understand these dependencies.

In this paper, we use the Born approximation (Born, 1933) to derive analytical expressions, which relate landmine and soil properties to the early-time response. In contrast to the well-established physical optics approach to early-time response modeling (Nag and Peters, 1998), the Born approximation is not restricted to smoothly curved objects and is able to account for internal reflections. Furthermore,

with the Born approximation studying arbitrary incident/scattering directions and target shapes is feasible, whereas the angle dependence of the Fresnel reflection coefficients introduces complexity that rules out analytical treatment of these cases with physical optics.

The derived expressions include the transfer function and the impulse response of a penetrable target embedded in a homogeneous lossy medium. We illustrate the expression of the target impulse response using a simple minelike target (a truncated circular cylinder) and compare its response predicted for a non-lossy host medium against that for a lossy host medium. To evaluate the usefulness of the responses predicted by the Born approximation, we simulated the response of the same minelike target for both the non-lossy and lossy case using a 3D finite-difference time-domain modeling program (Mur, 2001). The simulated responses are compared against the predicted responses followed by a brief discussion of the observed differences. We then propose two phenomenologically motivated modifications to the derived target impulse response expression and show that they significantly improve the fit of the predicted response to the simulated response. A general discussion of the results is given at the end of the paper.

APPROXIMATION OF THE EARLY-TIME RESPONSE OF A BURIED PENETRABLE TARGET

In the following, we will derive expressions describing the early-time response of a penetrable target embedded in an unbounded homogeneous lossy medium and illuminated by a uniform plane wave. In order to make analytical treatment tractable, we make use of the Born and far-field approximations. For further simplicity we will only analyze scattering in the direction opposite to the incident direction, i.e. a monostatic configuration is assumed. A schematic illustration of the configuration we consider is given in figure 1.

The host medium is characterized by the impedivity $\hat{z} = i\omega\mu_0$ and the admittivity $\hat{y} = i\omega\varepsilon + \sigma$, where ω denotes angular frequency, μ_0 is the vacuum magnetic permeability, and ε and σ are the medium's dielectric permittivity and conductivity. The target is described by the permittivity distribution $\varepsilon_t(\boldsymbol{x})$ and the conductivity distribution $\sigma_t(\boldsymbol{x})$ and hence constitutes an admittivity contrast $\delta\hat{y}(\boldsymbol{x}) = \hat{y}_t(\boldsymbol{x}) - \hat{y}$. The target's permeability is assumed to be equal to that of the host medium, i.e. μ_0. Without loss of generality, we further assume that the incident wave travels in the positive *z*-direction and that the

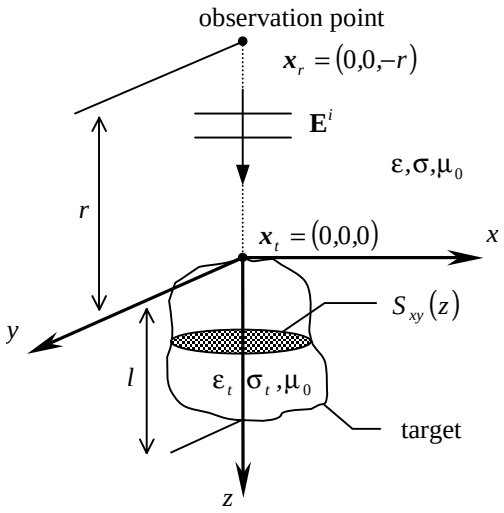

Figure 1: A target embedded in an unbounded homogeneous medium is illuminated by a uniform plane wave.

target is located at the origin of the coordinate system. Thus, in the frequency domain the incident field can be written as

$$\mathbf{E}^i(\boldsymbol{x}) = \mathbf{E}^i(\boldsymbol{x}_t)e^{-ikz} \quad , \tag{1}$$

where $k = \sqrt{-\hat{z}\hat{y}}$ is the wavenumber associated with the host medium and $\boldsymbol{x}_t$ refers to the target location.

The starting point of the derivation is the volume integral equation

$$\mathbf{E}^s(\boldsymbol{x}_r) = \iiint_{\text{target}} \tilde{\mathbf{G}}(\boldsymbol{x}_r, \boldsymbol{x})\mathbf{J}^s(\boldsymbol{x})\,dxdydz \tag{2}$$

(Oristaglio and Spies, 1999), which relates the equivalent scattering current distribution $\mathbf{J}^s(\boldsymbol{x})$ within the target to the scattered electric field at the observation point $\mathbf{E}^s(\boldsymbol{x}_r)$. The equivalent scattering current accounts for the target admittivity contrast and is defined as

$$\mathbf{J}^s(\boldsymbol{x}) = \delta\hat{y}(\boldsymbol{x})\left(\mathbf{E}^i(\boldsymbol{x}) + \mathbf{E}^s(\boldsymbol{x})\right) \tag{3}$$

The quantity $\tilde{\mathbf{G}}(\boldsymbol{x}_r, \boldsymbol{x})$ is the electric tensor Green's function. Its ij^{th} element determines the contribution of the j^{th} component of $\mathbf{J}^s(\boldsymbol{x})$ to the i^{th} component of $\mathbf{E}^s(\boldsymbol{x}_r)$. The full expression for the tensor Green's function for an unbounded homogeneous lossy medium can be found in Ward and Hohmann (1987, p. 181) and hence will not be repeated here.

We proceed by assuming that the target is a weak scatterer, i.e. the admittivity contrast $\delta\hat{y}(\boldsymbol{x})$ is low. In this case the

scattered field $\mathbf{E}^s(\boldsymbol{x})$ inside the target can be neglected in equation 3, leading to a linear relationship between the incident field and the scattered field at the observation point:

$$\mathbf{E}^s(\boldsymbol{x}_r) = \iiint_{\text{target}} \tilde{\mathbf{G}}(\boldsymbol{x}_r, \boldsymbol{x}) \delta\hat{y}(\boldsymbol{x}) \mathbf{E}^i(\boldsymbol{x}) dxdydz \ . \qquad (4)$$

Equation 4 is referred to as the Born approximation. Substituting equation 1 for the incident field, equation 4 becomes

$$\mathbf{E}^s(\boldsymbol{x}_r) = \left(\iiint_{\text{target}} e^{-ikz} \delta\hat{y}(\boldsymbol{x}) \tilde{\mathbf{G}}(\boldsymbol{x}_r, \boldsymbol{x}) dxdydz \right) \mathbf{E}^i(\boldsymbol{x}_t) \ . \qquad (5)$$

Further simplification can be achieved by using the far-field approximation of the tensor Green's function

$$\tilde{\mathbf{G}}(\boldsymbol{x}_r, \boldsymbol{x}) \approx -\hat{z} \frac{e^{-ik(r+z)}}{4\pi r} \begin{bmatrix} 1 & 0 & 0 \\ 0 & 1 & 0 \\ 0 & 0 & 0 \end{bmatrix} , \qquad (6)$$

which requires that all of the following three criteria are satisfied:

$$|kr| >> 1 \ , \qquad (7)$$

$$\frac{x}{r}, \frac{y}{r}, \frac{z}{r} << 1 \quad \text{for all } (x,y,z) \in \text{target} \qquad (8)$$

and

$$r \geq \frac{2D^2}{\lambda} \qquad (9)$$

(Balanis, 1989). Here r denotes the distance between the observation point and the target, D is the maximum dimension of the target and λ is the wavelength. Applying the far-field approximation to equation 5 and integrating over x and y, we obtain the wanted expression for the early-time response of the target in the frequency domain

$$\mathbf{E}^s(\boldsymbol{x}_r) = \frac{e^{-ikr}}{2\sqrt{\pi} r} H_I(\omega) \begin{bmatrix} 1 & 0 & 0 \\ 0 & 1 & 0 \\ 0 & 0 & 0 \end{bmatrix} \mathbf{E}^i(\boldsymbol{x}_t) \qquad (10)$$

with

$$H_I(\omega) = -\frac{\hat{z}}{2\sqrt{\pi}} \int_{z=0}^{l} e^{-i2kz} \overline{\delta\hat{y}}(z) S_{xy}(z) dz \ . \qquad (11)$$

The function $S_{xy}(z)$ describes the transverse cross-sectional area of the target (see figure 1) and the function $\overline{\delta\hat{y}}(z)$ is the average admittivity contrast over $S_{xy}(z)$. The parameter l refers to the length of the target measured along the z-axis. The first term on the right-hand side of equation 10 simply represents the phase shift, propagation loss and geometrical spreading loss associated with the one-way propagation from the target to the observation point. The quantity $H_I(\omega)$ is the target transfer function, which is independent of the distance to the observation point. The matrix term in equation 10 reflects the fact that the radial component of the scattered field vanishes in the far-field.

Finally, let us rewrite the early-time response of the target given by equations 10 and 11 in the time-domain. Substituting $z = vt/2$, equation 11 implies that the target impulse response is

$$h_I(t) = -\frac{\mu_0 v}{4\sqrt{\pi}} \left[\frac{\partial^2}{\partial t^2} \left(e^{-\alpha vt} \overline{\delta\varepsilon}\left(\frac{vt}{2}\right) S_{xy}\left(\frac{vt}{2}\right) \right) + \frac{\partial}{\partial t} \left(e^{-\alpha vt} \overline{\delta\sigma}\left(\frac{vt}{2}\right) S_{xy}\left(\frac{vt}{2}\right) \right) \right] \qquad (12)$$

where v and α are the wave velocity and the attenuation in the host medium, and $\overline{\delta\varepsilon}(z)$ and $\overline{\delta\sigma}(z)$ are the average permittivity and conductivity contrasts over $S_{xy}(z)$. The time-domain equivalent of equation 10 is given by

$$\mathbf{e}^s(\boldsymbol{x}_r, t) = \frac{e^{-\alpha r}}{2\sqrt{\pi} r} \delta\left(t - \frac{r}{v}\right) \otimes h_I(t) \otimes \begin{bmatrix} 1 & 0 & 0 \\ 0 & 1 & 0 \\ 0 & 0 & 0 \end{bmatrix} \mathbf{e}^i(\boldsymbol{x}_t, t) \qquad (13)$$

where $\otimes$ denotes convolution and $\delta(t)$ is the delta function.

Before presenting some example target impulse responses as predicted by equation 12, two characteristics of the derived early-time response expressions are worth pointing out. First, as a result of the Born and far-field approximations, equations 10 through 13 do not account for depolarization phenomena. This suggests that they are more suited for describing the scattering behavior of rotationally symmetric targets for which the scattered fields exhibit no cross-polar component (Carin *et al.*, 1999). Second, it should be noted that the target transfer function expression is more general than the impulse response expression, since the velocity and attenuation have to be assumed frequency independent to permit the transformation of equations 10 and 11 into the time-domain. This assumption is valid if the polarization losses are negligible and the conduction loss term $\sigma(\varepsilon_0 \omega)^{-1}$ is smaller than one (Roth *et al.*, 2001); ε_0 denotes the vacuum permittivity.

Target Impulse Response Examples

Figure 2 shows two examples of target impulse responses predicted by equation 12. As a target we chose a truncated circular cylinder oriented such that its rotational symmetry axis runs parallel to the *z*-axis, i.e. the normal incidence/backscatter response was evaluated. The target has a diameter of 10 cm and a height of 4 cm, similar to a PMA-3 mine. The target was given a relative dielectric permittivity of 2.8 and a zero conductivity, which are typical for plastics and explosives. We considered both a non-lossy (figure 2a) and a lossy host medium (figure 2b). For the non-lossy case, we selected a host medium relative permittivity of 4 and a zero conductivity. These values are representative for dry sand. For the lossy case, the conductivity was increased to 30 mS/m, while the relative permittivity remained set to 4. In both cases the peaks at around 0 ns relate to backscatter from the top of the target whereas the peaks at around 0.525 ns relate to backscatter from the bottom of the target. From figure 2a we can see that the target permittivity contrast is predicted to differentiate the waveform of the incident field. Furthermore, we observe two clear differences between the non-lossy and the lossy target impulse response. First, the losses add two smaller peaks to the impulse response as a result of the conductivity contrast term in equation 12. And second, the peaks at around 0.525 ns are "attenuated".

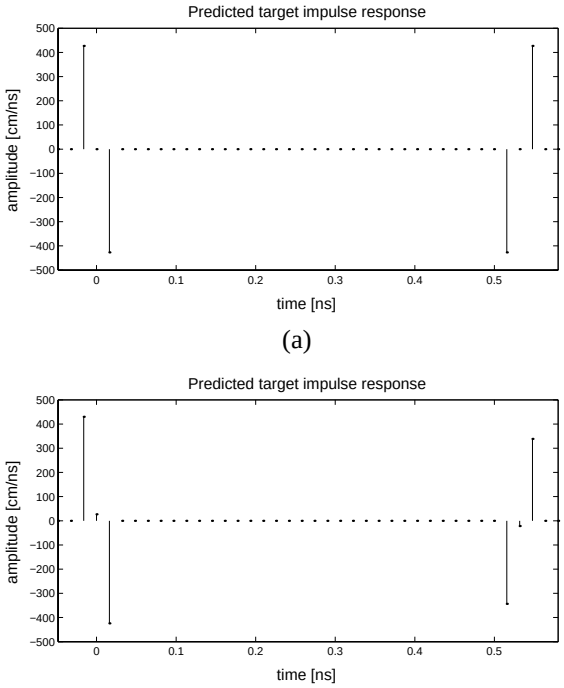

(a)

(b)

Figure 2: Normal incidence/backscatter impulse response of the example target as predicted by eq. 12 given

(a) the non-lossy host medium ($\varepsilon_r = 4$, $\sigma = 0$)

(b) the lossy host medium ($\varepsilon_r = 4$, $\sigma = 30$ mS/m).

THREE-DIMENSIONAL FDTD MODELING

For comparison, we simulated the response of the example target for the two host media (non-lossy and lossy) using a 3D FDTD modeling program. The program uses a total field formulation and allows for plane wave excitation of the computational domain through the use of total field absorbing boundary conditions (Mur, 1998). Scattered fields were obtained by simply repeating the simulations without the target and then subtracting the so-obtained incident field data from the total field data. The incident field data can also be used to roughly estimate the accuracy of the FDTD simulations by comparing it to the theoretical plane wave field. Doing so, we observed an amplitude error accumulation of about 1 % per 10 cm the plane wave traveled through the domain of computation.

A linear polarization in the *x*-direction was selected for the incident plane wave and all simulated responses shown in this paper refer to the *x*-component of the scattered field. For the time function of the incident plane wave we chose a Ricker wavelet (2^{nd} derivative of a Gaussian pulse) with a peak amplitude frequency of 1.5 GHz and a peak amplitude of 10000 (nominal value). The energy spectrum of this wavelet is such that the velocity and attenuation in the lossy host medium can be assumed frequency independent. Furthermore, from the spectrum information and equations 7 through 9, it follows that the far-field approximation of the tensor Green's function can safely be assumed valid at distances greater than 50 cm from the example target.

Figure 3 shows the simulated response at a distance of 60 cm from the target for the non-lossy and lossy host medium, respectively. Since the velocity and attenuation in the lossy host medium can be assumed frequency independent, the difference in shape between the two responses can be attributed to a difference in target impulse response.

In figure 4 the same two simulated responses are plotted against those predicted by our approximate early-time response model (equations 12 and 13). In order to account for any simulation errors that accumulate while the incident field propagates to the target, we used the simulated incident field at the target location and not the theoretical plane wave field for the predictions. Considering that the incident wave has an initial amplitude of 10000, we observe that for both the non-lossy and the lossy case the amplitudes

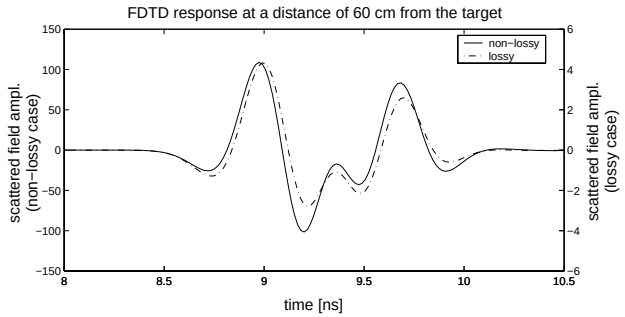

Figure 3: Simulated response of the example target for the non-lossy ($\varepsilon_r = 4, \sigma = 0$) and the lossy ($\varepsilon_r = 4, \sigma = 30$ mS/m) host medium.

of the first three signal peaks are well predicted as is the general shape of the response, i.e. the number of signal peaks. However, some of the remaining peaks are not accurately predicted in both time and amplitude. Note that the amplitude mismatch is higher for the non-lossy case than for the lossy case.

The mismatch between the simulated and predicted responses can be explained by the fact that according to the Born approximation electromagnetic energy (incident and scattered) propagates through the target at the velocity of the host medium. Furthermore, the Born approximation does not account for transmission losses at the surface of the target. Consequently, neglecting wave attenuation effects, backscatter from the bottom of the target will be predicted as being equally strong in amplitude as backscatter from the top of the target. Based on these considerations we have introduced some phenomenological modifications to the target impulse response given by equation 12. First, we replaced the velocity and attenuation of the host medium, v and α, by the averages $(v+v_t)/2$ and $(\alpha+\alpha_t)/2$, where v_t and α_t refer to the velocity and the attenuation in the target. This modification honors the fact that the incident and scattered fields propagate through as well as along the outside of the target. As a second modification, we multiplied all peaks in the predicted target impulse response that relate to backscatter from the bottom of the example target by the factor $\varepsilon_t / \varepsilon = 0.7$. Figure 5 shows the target responses predicted by this phenomenologically modified model and their simulated counterparts. We find that for both the non-lossy and the lossy case the predicted responses nicely fit the simulated responses in time as well as amplitude.

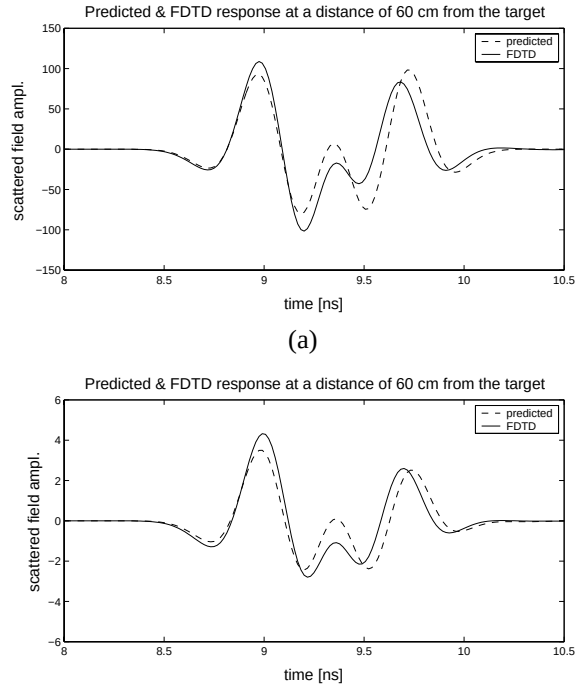

Figure 4: Predicted (eqs. 12 & 13) and simulated response of the example target given
(a) the non-lossy host medium ($\varepsilon_r = 4, \sigma = 0$)
(b) the lossy host medium ($\varepsilon_r = 4, \sigma = 30$ mS/m).

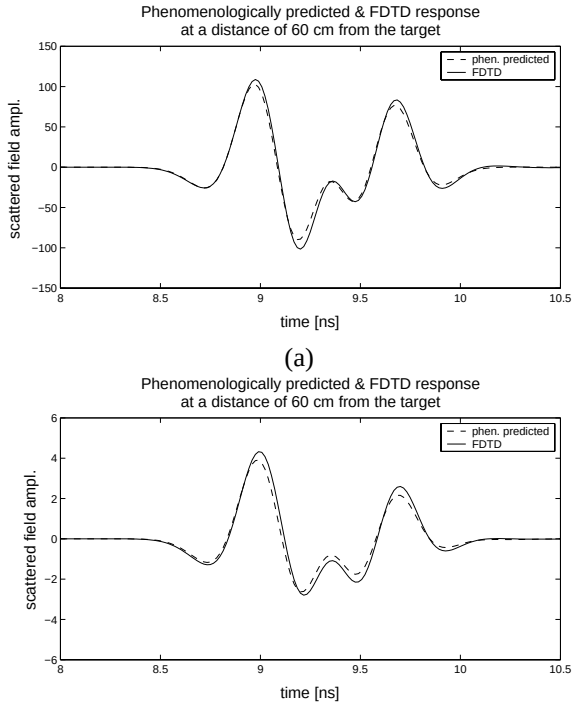

Figure 5: Phenomenologically predicted and simulated response of the example target given
(a) the non-lossy host medium ($\varepsilon_r = 4, \sigma = 0$)
(b) the lossy host medium ($\varepsilon_r = 4, \sigma = 30$ mS/m).

DISCUSSION

We have developed simple analytical expressions for the early-time radar response of a penetrable target embedded in a homogeneous lossy medium. Comparing predicted responses of the example target against FDTD simulated responses demonstrates that these expressions have the capability to correctly model not just the general shape of the target response, but also the dependency of the target impulse response on the conductivity of the host medium. Knowing how the target impulse response changes as a function of the host medium properties is crucial for the identification of buried targets under varying soil conditions.

Clearly, for the application to landmine identification with GPR, the presented early-time response expressions require further verification (numerical and experimental) with different incident/backscatter directions, target shapes/sizes and admittivity contrasts, and ultimately the extension to the near-field. This will be the subject of future research.

ACKNOWLEDGEMENTS

This research was funded by the Dutch Technology Foundation STW, applied science division of NWO. The authors wish to thank G. Mur for making his FDTD code available to them.

REFERENCES

Balanis, C.A., 1989, *Advanced Engineering Electromagnetics*, Wiley, 941p.

Baum, C.E., Ed., 1998, *Detection and Identification of Visually Obscured Targets*, Taylor & Francis, Philadelphia, 434p. + CD

Born, M., 1933, *Optik*, Springer, Berlin, 591p.

Carin, L., Geng, N., McClure, M., Sichina, J. and Nguyen, L., 1999, Ultra-Wide-Band Synthetic-Aperture Radar for Mine-Field Detection, *IEEE Antennas & Propagation Magazine*, Vol. 41, No. 1, p. 18-33

Chen, C.-C. and Peters, L., 1997, Buried Unexploded Ordnance Identification via Complex Natural Resonances, *IEEE Trans. Antennas Propagat.*, Vol. 45, No. 11, p. 1645-1654

Kostylev, A.A., 1994, Radar Target Characteristics for Wide-Band and Ultrawide-Band Signals, *in* Astanin, L.Y., Kostylev, A.A., Zinoviev, Y.S., Pasmurov, A.Y., Eds., *Radar Target Characteristics: Measurements and Applications*, CRC Press, Boca Raton, FL, p. 47-76

Mur, G., 1998, Total-Field Absorbing Boundary Conditions for the Time-Domain Electromagnetic Field Equations, *IEEE Trans. Electromagn. Compat.*, Vol. 40, No. 2, p. 100-102

Mur, G., 2001, *FDTD3D: The C++ Finite-Difference Code for Electromagnetic Fields in Three Dimensions and Time*, IRCTR and Laboratory of Electromagnetic Research, Delft University of Technology, The Netherlands

Nag, S. and Peters, L., 1998, Ramp Response Signatures for Dielectric Targets, *Proc. SPIE*, Vol. 3392, Detection and Remediation Technologies for Mines and Minelike Targets III, April, 1998, Orlando, FL, p. 703-713

Oristaglio M. and Spies B., Eds., 1999, *Three-Dimensional Electromagnetics*, Geophysical Development Series: Vol. 7, Soc. Expl. Geophys., 709p.

Roth, F., van Genderen, P. and Verhaegen, M., 2001, Analysis of the Influence of Mine and Soil Properties on Features extracted from GPR Data, *Proc. SPIE*, Vol. 4394, Detection and Remediation Technologies for Mines and Minelike Targets VI, April, 2001, Orlando, FL, p. 428-439

Ward, S. H., and Hohmann, G.W., 1987, Electromagnetic Theory for Geophysical Applications, *in* Nabighian, M. N., Ed., *Electromagnetic Methods in Applied Geophysics Vol. I*: *Theory*, Investigations in Geophysics Series: no. 3, Soc. Expl. Geophys., p. 130-311